Arch. Mech., 44, 4, pp. 391–408, Warszawa 1992

On the yield surface behavior in the case of proportional cyclic loading histories

W. TRĄMPCZYŃSKI and E. SENDER (WARSZAWA)

EXPERIMENTAL RESULTS concerning the yield surface evolution in the case of proportional cyclic loading histories are reported. They were obtained for 18G2A steel, at room temperature, using one specimen technique, where the "offset" yield definition was assumed to be $\eta = 0.0005$. The experiments were carried out on thin-walled tubes under cyclic tension-compression and opposite torsion with constant strain rate $\dot{\varepsilon}_e = 3.4^{*}10^{-4}\ s^{-1}$. The influence of former plastic strain history on the yield surface shape and magnitude in steady cyclic state is shown. It was found that the yield surface in the $\sigma_x, \sqrt{3}\tau_{xy}$ space can be described by an ellipse, within +8%; −6% accuracy, independently of the former plastic strain history.

1. Introduction

ALTHOUGH it is well established that, for majority of metals in the virgin state, the Huber–Mises potential can be used for the yield surface description, the surface shape after plastic prestraining is still the subject of experimental examination. In spite of the fact that such experiments have been carried out since a long time [1–7], their results are still difficult to evaluate. It is mainly due to:

a limited amount of experimental data,

dependence of the yield surface shape on the applied experimental technique.

Because of technical difficulties connected with obtaining the well defined and homogeneous three-dimensional stress state, experiments are usually conducted under plane stress conditions. The different ways of specimen loading can be represented by planes intersecting the Huber–Mises potential [8, 9]. The ellipses obtained visualize the stress-state which is realized using different experimental techniques as: tension–torsion, tension–internal pressure, tension–torsion–internal pressure and torsion of thin tubular specimens [Fig. 1]. Any of the testing methods mentioned above gives only a limited amount of information concerning the material behavior in the whole stress space, and their results have to be treated as complementary. It can be assumed that tension–torsion tests of thin tubular specimens are mostly used. In such a case the yield surface determination method is schematically shown in Fig. 2. The yield surface is defined by experimental determination of several yield points. The specimens are loaded with different σ_x, τ_{xy} ($\varepsilon_x, \gamma_{xy}$) ratios up to the yield limit defined usually as the state of stress corresponding to a certain plastic strain value [1]. Such a technique can be realized in two ways:

the entire yield surface is determined using one specimen and the consecutive yield points are defined by slight surface "punching",

every yield point on the yield surface is determined using one specimen.

The first technique, mentioned above, can be applied when the yield limit is defined as that corresponding to a small amount of plastic strains. It is due to the fact that every yield surface "punch" adds some plastic strains to the plastic loading history. Hence, determination of several points can disturb this history. Thus the amount of yield surfaces

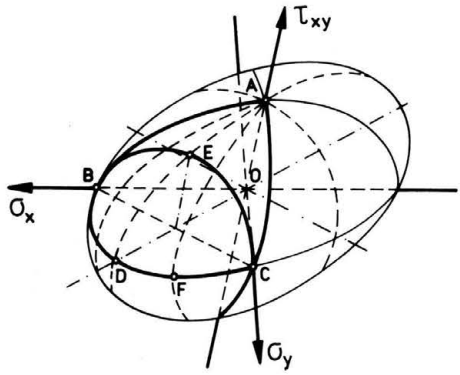

FIG. 1. Different ways of loading (usually used in experiments) shown as intersection of Huber–Mises surface in the plane stress with appropriate planes corresponding to the way of loading, AB or AC – tension-torsion of thin tubular specimens, BDC – tension-internal pressure of thin tubular specimens or tension of cruciform specimens, AD or AF – tension-torsion-internal pressure of thin tabular specimens, point A – torsion of thin tubular specimen.

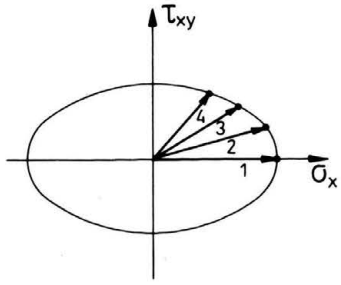

FIG. 2. The yield surface determination.

defined during the loading program is limited, and the obtained data can prove to be insufficient for the detection of the material parameter evolution in the case of more complicated loading histories.

The second technique is expensive (large number of specimens is needed) and all the data obtained contain a scatter due to different material properties of different specimens.

In both cases the yield surface determination is a laborious, technically difficult and costly task. Although, when computer-controlled testing machines are used (in the case of more complicated loading histories, when the yield surface has to be defined in several points), it is a very complicated and expensive program to be carried out.

Evaluation of experimental results concerning the yield surface determination is not simple due to the lack of a unique experimental definition of the yield limit. The definitions used embrace the vast range of material behavior, starting from the elastic, linear strain limit, through various apparent plastic limits, up to the stress corresponding to the fully developed stage of plastic deformation [1]. The yield surfaces established for such a variety of definitions are different and hardly comparable. For example, in Fig. 3 there are shown the yield surfaces for copper after 17% of shear, obtained for different yield definitions [10]. Their shapes are quite different and for example "the cross effect"

changes from 70% in the case of "small" offset yield definition to 15% in the case of back extrapolation technique, when the yield surface coincides with that of the Tresca yield limit.

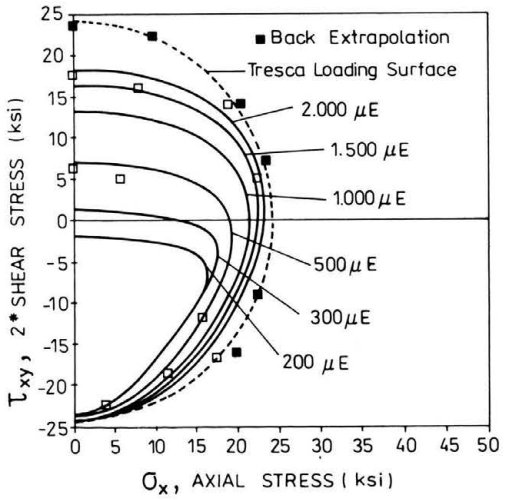

FIG. 3. Subsequent yield surfaces in the σ_x, $2\tau_{xy}$ space for various offset strains yield definitions in the case of copper prestrained by torsion up to 17% [10].

In addition, evaluation of the results is difficult due to two different methods of determination of the yield surfaces: in some experiments they are determined after complete unloading of the material, and in other cases the surfaces are analyzed after partial unloading of the specimen. The yield surfaces found by means of these two methods differ from each other considerably, in particular when "small" yield limit definitions are used.

Independently of the differences resulting from the application of various methods of the yield point determination and various testing techniques, it is observed that the yield surfaces undergo complex transformations due to inelastic deformations. Not only the size but also the position, orientation and shape strongly varies for more complex loading. Such effects are well pronounced specially for "small" offset yield definitions.

Not always such a complicated material behavior is observed. In [5, 6] it is reported that the yield surface for SUS 304 Stainless Steel, under proportional and non-proportional loading, can be described, to within a certain accuracy, by an elliptical surface (in σ_x, τ_{xy} space). Its maximum radius is kept constant throughout all the history, starting from the virgin state when it coincides with the Huber–Mises yield surface radius [Fig. 4]. The yield surface distortion due to the plastic straining history consist only in changing of its second semi-axis. The experiments were carried out [5, 6] under tension- compression-torsion of thin tubular specimens at room temperature, using the 50 μm/m offset strain criterion for the yielding probed at the current center of the yield surface.

Similar shapes of yield surfaces were detected also for 18G2A steel tested at room temperature. The experiments were carried out [11] on thin tubes, under tension-compression and torsion, for monotonic and proportional loading histories using the 500 μm/m offset

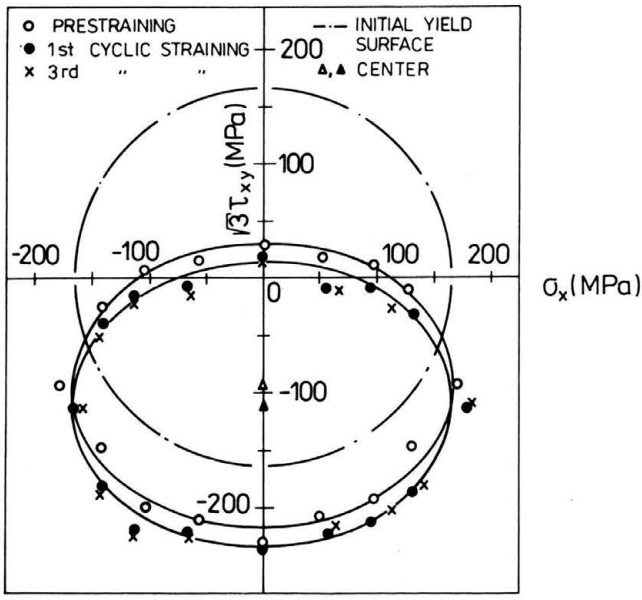

FIG. 4. SUS 304 subsequent yield surfaces during cyclic torsion straining ($\gamma_{xy}/\sqrt{3} = 1\%$) [5].

strain criterion for the yielding probed at the current center of the yield surface. Although the detected yield surfaces shows their "flattening" in the direction opposite to prestraining, they can be described by ellipses, within the $+8\%$; -6% accuracy. It was also found that semi-axes "a" and "b" of the ellipse (defined in the way shown in Fig. 7) change simultaneously during the whole straining history. These results were obtained by keeping all the time the same loading direction (all the monotonic loading and cyclic loading experiments were carried out either for tension-compression or for torsion).

The results presented in this paper show the influence of different loading histories on the material yield surface behavior (at steady state), under cyclic tension-compression and opposite torsion, in the case when loading directions do not coincide. For example, the influence of monotonic tensile loading on cyclic opposite torsion, or the effect of cyclic tension-compression on cyclic opposite torsion material yield surface behavior (at steady state) is reported. Then, these experimental results and those reported in [11] are summarized, and conclusions concerning the 18G2A Steel yield surface behavior under cyclic loading are drawn.

The results obtained can be treated as complementary to those presented in [11 and 13]. Results of a broad experimental program for 18G2A and 21CrMoV57, including low cyclic and monotonic loading, are shown in [13]. The technique of successive unloadings were used and the evolution of parameters Π_1 and Y_1 was studied for quite complicated loading histories. Assuming the Huber–Mises yield criterion, the Π_1 and Y_1 parameters describe the position of the yield surface center and magnitude of its radius, and the evolution of kinematic and isotropic hardening can be investigated. In [11] a similar experimental program for 18G2A Steel was performed and the yield surface evolution was studied using the one specimen "punching" technique. The results obtained can be compared with that resulting from the successive unloading technique [13]. In this paper the

results of a similar experimental program (the one specimen "punching" technique being also used) for the same material are presented, but in the case when loading directions do not coincide. Hence, the experimental results presented in the three papers give a broad information about the 18G2A Steel yield surface behavior in the case of monotonic and cyclic loading.

2. Experimental results

The experimental program was carried out at room temperature on thin tubes (outer diameter 22,5 mm, wall thickness 1.25 mm) made of 18G2A steel. Tension-compression and opposite torsion cyclic programs were performed using the Institute of Mechanics 1 of Bochum University facilities, described in [12]. All programs were performed with a constant effective strain rate $\dot{\varepsilon}_e = 3.4 \cdot 10^{-4}\ s^{-1}$, and the actual stress versus the logarithmic plastic strain were calculated and plotted.

The yield points were defined by the offset definition $\eta = 0.0005$ for the yielding probed at the current center of the yield surface which was detected in the way described in [12]. In the chosen moment of plastic strain history the stress deviator value S_{ij} was recorded, the straining direction was reversed and the second yield point on the yield surface S_{ij}^R was found, using $\eta = 0.0005$ offset technique (in the case of complex stresses the σ_e versus ε_e curves were used). Then the center $O = (S_{ij} + S_{ij}^R)/2$ was determined and other points on the yield surface were searched in the way shown in Fig. 5a, always starting from point 0.

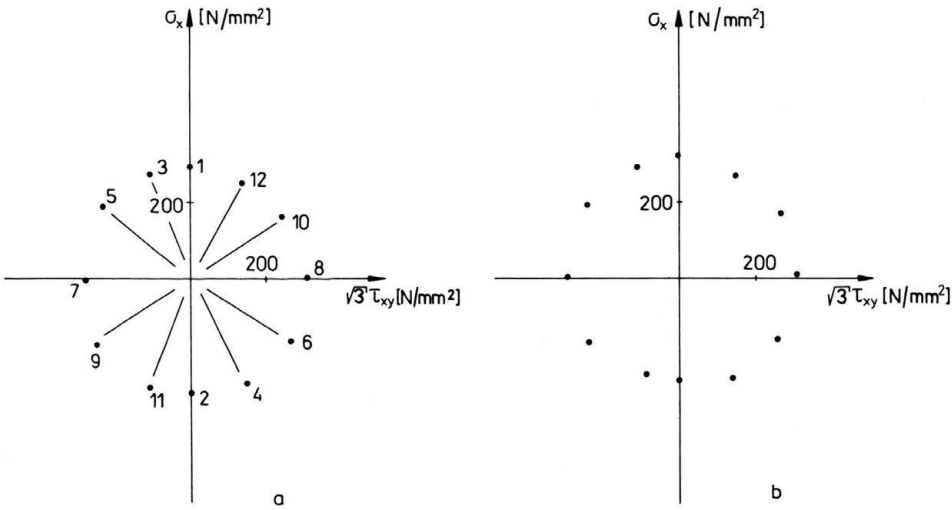

FIG. 5. The virgin material yield surface determined in two following "punching" procedures (Fig. 5a and Fig. 5b).

Due to the instable behavior of the σ_x versus ε_x^p curve for this material, all the specimens were primarily prestrained up to $\varepsilon_e^p = 0.003$ in tension, compression and opposite

torsion. Hence, all the specimens were primarily preloaded with $\varepsilon_e^p = 1.2\%$. Such specimens are called in this paper the "virgin" ones.

As it was mentioned before, in the case of the one specimen technique, every yield point determination adds some plastic strain value due to the yield definition. For the presented experimental program the "offset" definition $\eta = 0.0005$ was assumed. Hence, detecting 12 separate yield points (Fig. 5a), the additional effective plastic strain of $\varepsilon_e^p = 0.006$ was imposed during every procedure of the yield surface determination. The influence of such a plastic strain increment on the shape of the yield surface is shown in Fig. 5 and Fig. 6. In both cases the yield surface was detected twice, one after the other, starting from the direction of tension. In Fig. 5a and 5b the yield surfaces obtained this way, in the case of the virgin material, are shown. Similar surfaces for the material prestrained by tension are presented in Fig. 6.

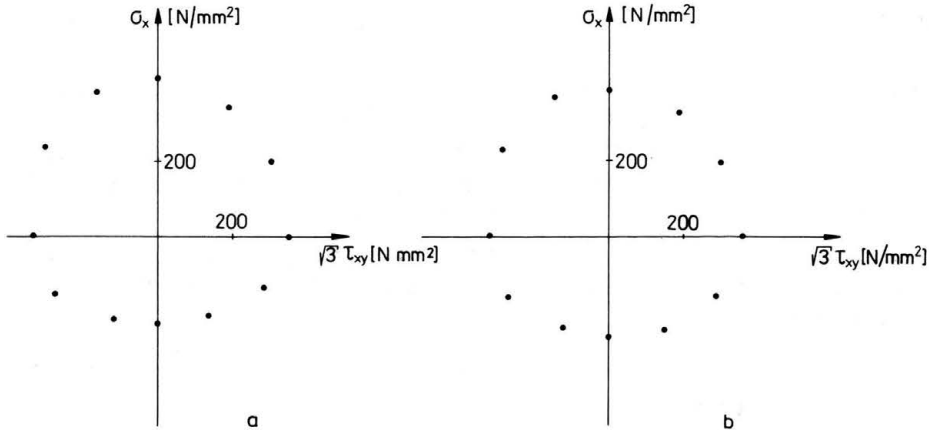

FIG. 6. The prestrained material yield surface determined in two following "punching" procedures (Fig 6a and Fig 6b).

It is seen that, although slight change in the yield surface position is recorded, its shape doesn't change.

Experiment 1. Monotonic loading under tension

The specimen was loaded by tension with the constant effective strain rate $\dot{\varepsilon}_e = 3.4 \times 10^{-4}\ s^{-1}$. The yield surface was determined for the virgin material and for the material prestrained up to $\varepsilon_x^p = 10\%$. The shape of the yield surface coincides with the Huber–Mises ones only in the case of virgin material (Fig. 7b-1). Then, a cross-effect is observed. The yield surface flattens in the direction "opposite" to the actual plastic strain and gets a "nose" in the direction of loading. The surface has no longer the center of symmetry, but it is symmetrical with respect to the actual straining direction. It is shown (Fig. 7b-2) that, even for such a considerable directional prestrain, the yield surface shape can be described by an ellipse with +8%, −6% accuracy. The broken lines shows the +8% and −6% ellipses. They were drawn in the following manner: at the beginning two main dimensions: a and b, were determined.

The first one (a) represents the yield surface dimension in the direction of loading ($a = [3/2(S_{ij} - S_{ij}^R)(S_{ij} - S_{ij}^R)]^{1/2}$; $a = [3/2(S_{ij}^1 - S_{ij}^2)(S_{ij}^1 - S_{ij}^2)]^{1/2}$; Fig. 7b-2); the second one (b) represents the yield surface dimension in the direction perpendicular to the main loading direction ($b = [3/2(S_{ij}^3 - S_{ij}^4)(S_{ij}^3 - S_{ij}^4)]^{1/2}$), starting from the middle point $O = (S_{ij} + S_{ij}^R)/2$. Having these two basic semi-axes (a, b — such ellipses are drawn by solid lines throughout the paper), the ellipses +8% and −6% were drawn (broken lines). The same technique was used in the case of all experimental data shown in Figs. 7–15.

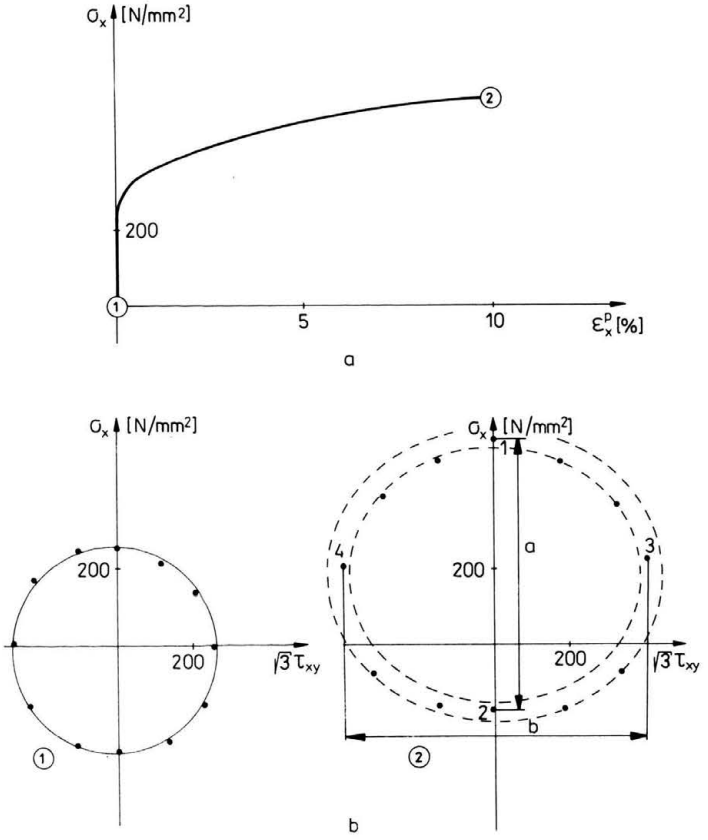

FIG. 7. Monotonic loading curve under tension and the yield surfaces determined for virgin and $\varepsilon_x^p = 10\%$ plastically prestrained material. a. The loading diagram. b. The yield surfaces measured in different moments of the loading history.

Experiment 2. Monotonic torsion ($\gamma_{xy}^p/\sqrt{3} = 5\%$) followed by cyclic torsion ($\gamma_{xy}^p/\sqrt{3} = \pm 0.5\%$)

The specimen was first cyclically loaded under opposite torsion ($\gamma_{xy}^p/\sqrt{3} = \pm 0.5\%$) until the stabilized loop was achieved, then monotonically twisted up to $\gamma_{xy}^p/\sqrt{3} = 5\%$, and then cyclically loaded under opposite torsion ($\gamma_{xy}^p/\sqrt{3} = \pm 0.5\%$) up to the stabilized loop (Fig. 8a). The yield surfaces were determined in three moments of the mentioned

loading history, and comparison between the yield surfaces before and after monotonic torsion was made (Fig. 8b). The yield surface resulted from the monotonic loading is larger than the cyclic one, but of similar shape and proportions (Fig. 8b-1 and Fig. 8b-2). Owing to the monotonic torsion it was expanded, and then reduced almost to the former dimensions due to the following cyclic loading, even when a small cyclic amplitude was applied. Only small memory effects of this prestrain are observed on subsequent yield surface dimensions, even if such a considerable prestrain was applied.

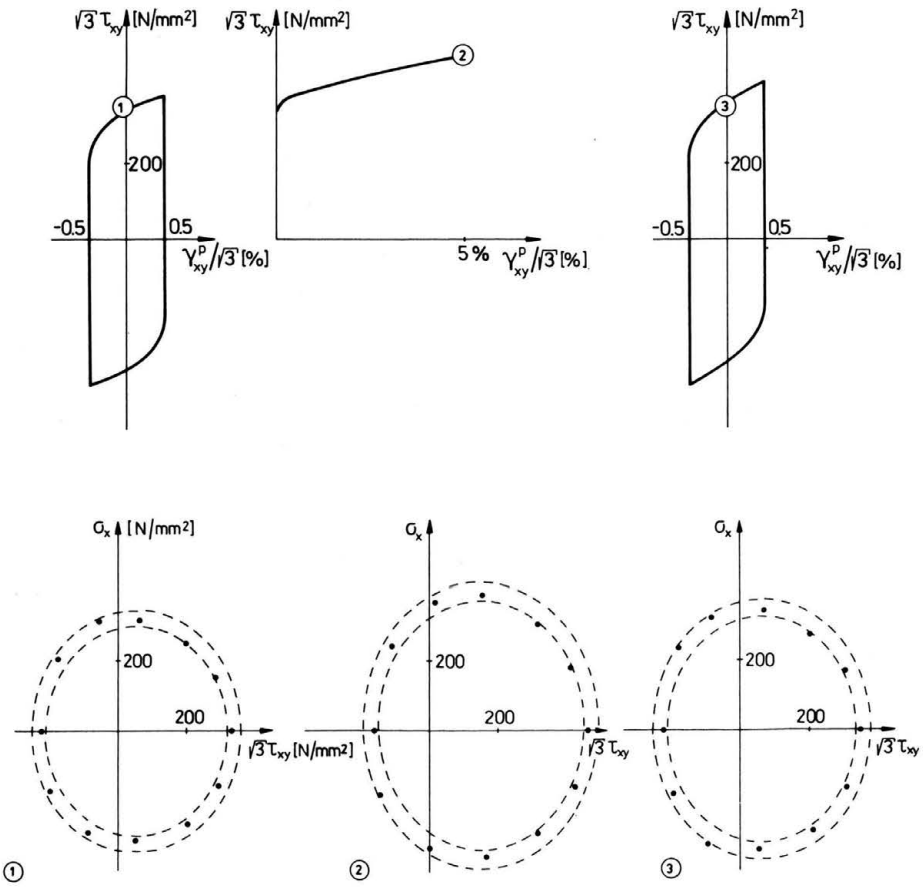

FIG. 8. Cyclic torsion ($\gamma^p_{xy}/\sqrt{3} = \pm - 0.5\%$) followed by monotonic torsion ($\gamma^p_{xy}/\sqrt{3} = 5\%$) and cyclic torsion ($\gamma^p_{xy}/\sqrt{3} = \pm 0.5\%$). a. The loading diagram. b. The yield surfaces measured in different moments of the loading history.

Experiment 3. Monotonic torsion ($\gamma^p_{xy}/\sqrt{3} = 4\%$) followed by cyclic tension-compression ($\varepsilon^p_x = \pm 0.5\%$)

The specimen was first cyclically loaded under tension-compression ($\varepsilon^p_x = \pm 0.5\%$) up to the stabilized loop, then monotonically twisted up to $\gamma^p_{xy}/\sqrt{3} = 4\%$ and then once more cyclically loaded by tension-compression ($\varepsilon^p_x = \pm 0.5\%$) (Fig. 9a). The yield surfaces were

determined in four moments of the mentioned loading history, and comparison between the yield surfaces before and after the monotonic torsion was made (Fig. 9b). As before (Experiment 2) the yield surface resulting from the monotonic loading is larger than the cyclic one, but of similar shape and proportions (Fig. 9b-2 and Fig. 9b-3). Because of monotonic torsion it was expanded, and then shrinked due to the following cyclic loading, but the former magnitude was not achieved. So, in the case when the cyclic direction was "perpendicular" to the monotonic one, some memory effects of this prestrain are observed on subsequent yield surface dimensions. These effects produce changes in the magnitude of the yield surface, while its shape remains almost constant.

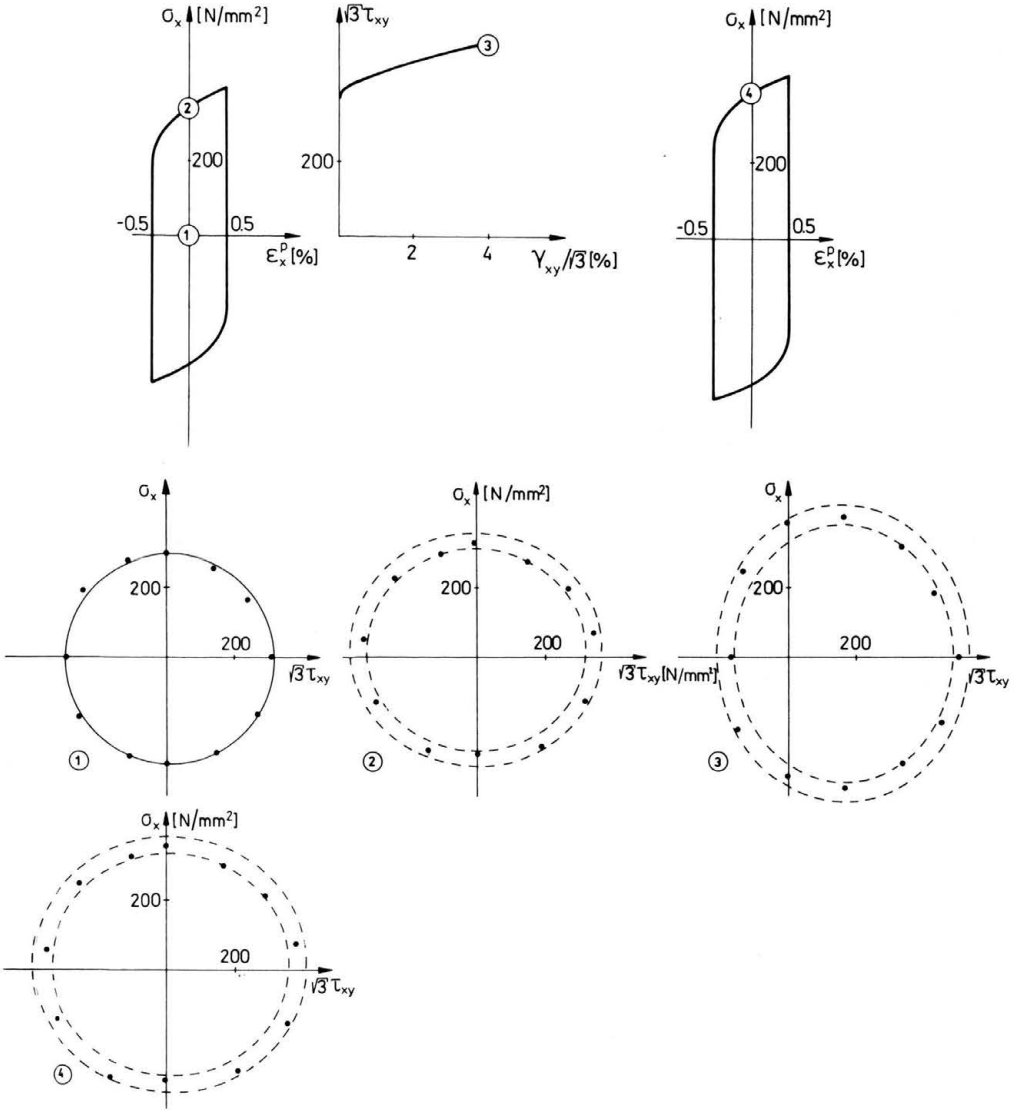

FIG. 9. Cyclic tension-compression ($\varepsilon_x^p = \pm 0.5\%$) followed by monotonic torsion ($\gamma_{xy}^p/\sqrt{3} = 4\%$) and cyclic tension compression ($\varepsilon_x^p = \pm 0.5\%$). a. The loading diagram. b. The yield surfaces in different moments of the loading history.

Experiment 4. Monotonic torsion ($\gamma_{xy}^p/\sqrt{3} = 5\%$) followed by cyclic tension-compression ($\varepsilon_x^p = \pm 0.75\%$) and then cyclic torsion ($\gamma_{xy}^p/\sqrt{3} = \pm 0.5\%$)

Experiment 4 was similar to the Experiment 3 and was performed to check the results obtained before. The specimen was first cyclically loaded under tension-compression ($\varepsilon_x^p = \pm 0.75\%$) up to the stabilized loop, then monotonically twisted up to $\gamma_{xy}^p/\sqrt{3} = 5\%$ and then once more cyclically loaded by the tension compression ($\varepsilon_x^p = \pm 0.75\%$) loading. Then cyclic opposite torsion loading $\gamma_{xy}^p/\sqrt{3} = \pm 0.5\%$ was applied (Fig. 10a). The yield surfaces were determined in four moments of the mentioned loading history, and comparison between the yield surfaces before and after the monotonic torsion was made (Fig. 10b). The yield surface is shown in Fig. 10b-A; it is the $\gamma_{xy}^p/\sqrt{3} = \pm 0.5\%$ opposite torsion cyclic surface for the virgin material. The results similar to those mentioned before are obtained. Certain memory effect of monotonic torque prestrain on the subsequent cyclic tension-compression yield surface dimensions is observed. Such effect is also detected when the loading is changed to the opposite torsion $\gamma_{xy}^p/\sqrt{3} = \pm 0.5\%$ (Fig. 10b-4; Fig. 10b-A).

Experiment 5. Cyclic opposite torsion ($\gamma_{xy}^p/\sqrt{3} = \pm 0.5\%$ and $\pm 1.0\%$) followed by cyclic tension-compression ($\varepsilon_x^p = \pm 1\%$) and opposite torsion $\gamma_{xy}^p/\sqrt{3} = \pm 0.5\%$

The specimen was first cyclically loaded under opposite torsion ($\gamma_{xy}^p/\sqrt{3} = \pm 0.5\%$) up to the stabilized loop, then the amplitude was changed to ($\gamma_{xy}^p/\sqrt{3} = \pm 1.0\%$). When the steady state was reached, the loading was changed to cyclic tension-compression ($\varepsilon_x^p = \pm 1\%$). Then, cyclic opposite torsion of $\gamma_{xy}^p/\sqrt{3} = \pm 0.5\%$ was applied (Fig. 11a). The yield surfaces were determined in five moments of the loading history mentioned above, and comparison between the yield surfaces was made (Fig. 11b). The yield surface resulted from the $\gamma_{xy}^p/\sqrt{3} = \pm 0.5\%$ cyclic torsion loading is shown in Fig. 11b-2. It can be no more described by the Huber–Mises potential (as in the case of a virgin material). Considerable cross-effect is observed but the surface is symmetrical with respect to the applied load direction. Then, because of the applied bigger cyclic amplitude, it grows up. As a result of tension-compression cyclic loading the yield surface becomes symmetrical to σ_x. Then, as a result of the following cyclic opposite torsion, it once more becomes symmetrical with respect to the τ_{xy} axis. Because of the applied smaller cyclic strain amplitude, it also shrinks to its former magnitude (Fig. 11b-2 and Fig. 11b-5). No memory effect is observed.

Experiment 6. Cyclic tension-compression ($\varepsilon_x^p = \pm 0.5\%$) followed by cyclic opposite torsion ($\gamma_{xy}^p/\sqrt{3} = \pm 1.5\%$) and then cyclic tension-compression and cyclic opposite torsion with the same amplitude ($\varepsilon_x^p = \pm 0.5\%$, $\gamma_{xy}^p/\sqrt{3} = \pm 0.5\%$)

A similar loading program as in Experiment 5 was carried out in Experiment 6. The specimen was first cyclically loaded under tension-compression ($\varepsilon_x^p = \pm 0.5\%$) up to the stabilized loop, and the loading was changed to opposite torsion with $\gamma_{xy}^p/\sqrt{3} = \pm 1.5\%$ amplitude. When the steady state was reached, the loading was changed to cyclic tension-compression ($\varepsilon_x^p = \pm 0.5\%$). Then, cyclic opposite torsion of the same amplitude was

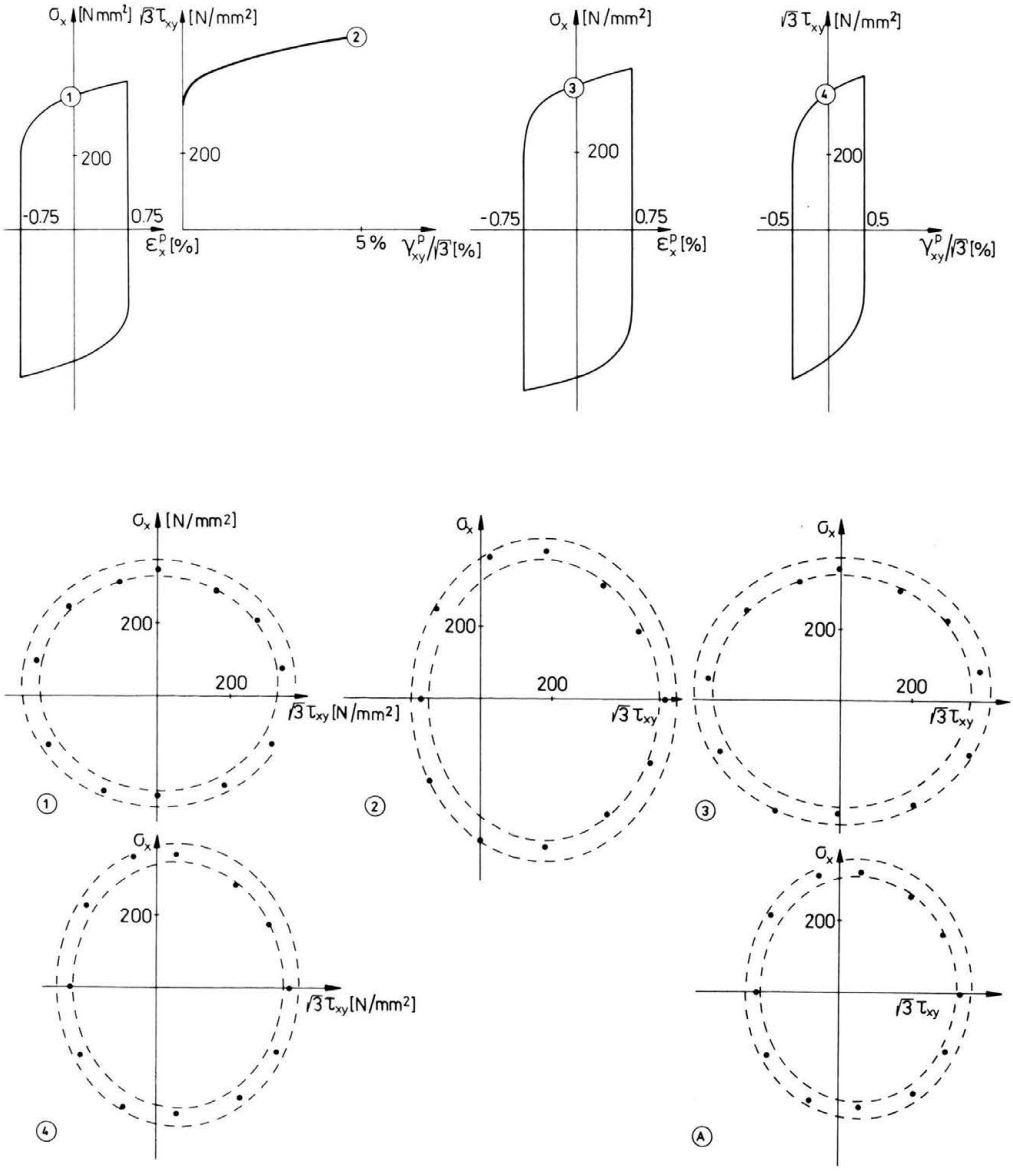

FIG. 10. Cyclic tension-compression ($\varepsilon_x^p = \pm 0.75\%$) followed by monotonic torsion ($\gamma_{xy}^p/\sqrt{3} = 5\%$), cyclic tension compression ($\varepsilon_x^p = \pm 0.75\%$) and cyclic torsion ($\gamma_{xy}^p/\sqrt{3} = \pm 0.5\%$). a. The loading diagram. b. The yield surfaces measured in different moments of the loading history.

applied (Fig. 12a). The yield surfaces were determined in four moments of the loading history mentioned above, and comparison between the yield surfaces was made (Fig. 12b). Although the yield surface resulting from the cyclic $\gamma_{xy}^p/\sqrt{3} = \pm 1.5\%$ torsion loading has a similar shape to that for the $\varepsilon_x^p = \pm 0.5\%$ cyclic tension-compression, it is larger and

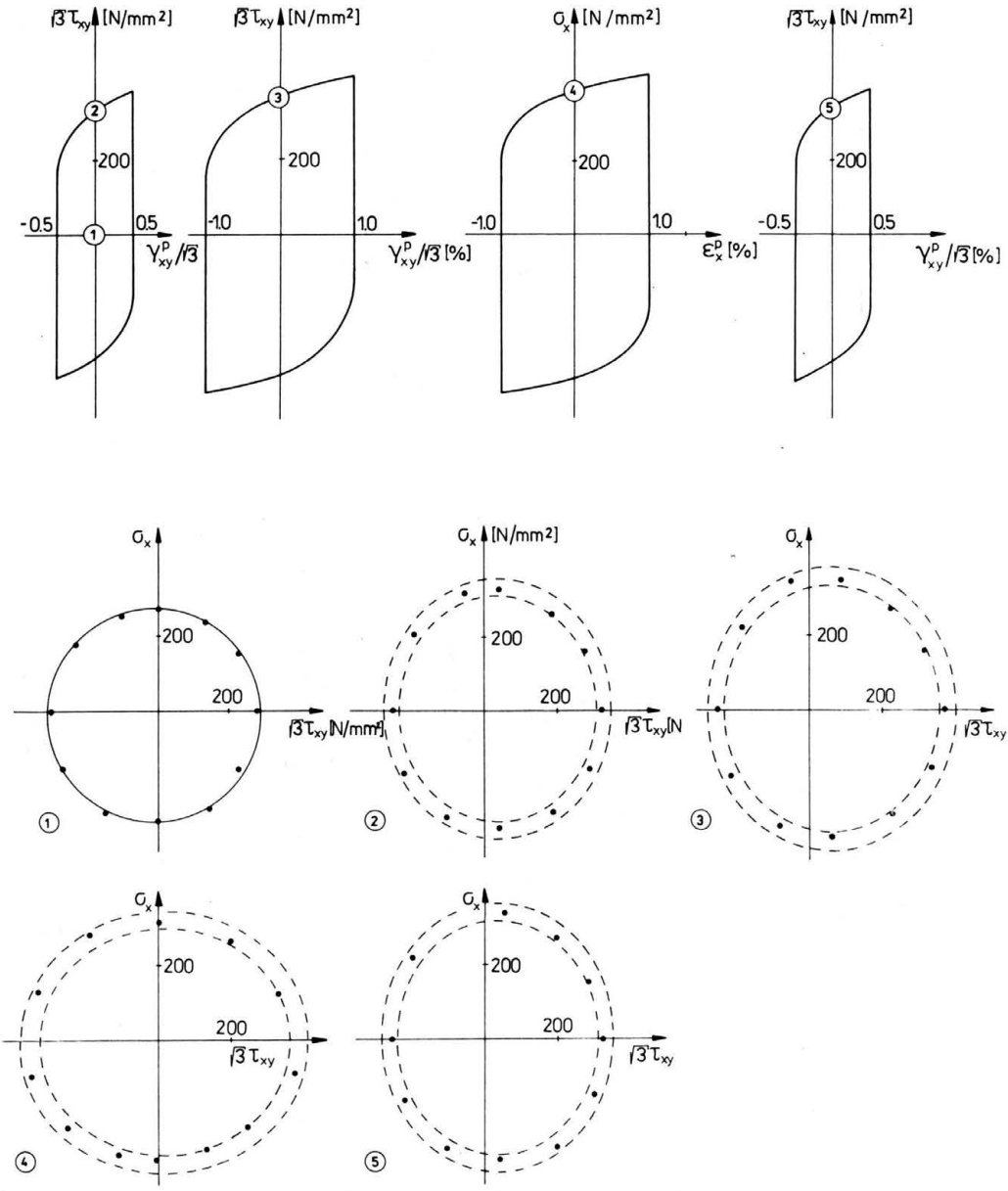

FIG. 11. Cyclic opposite torsion ($\gamma^p_{xy}/\sqrt{3} = \pm 0.5\%$ and $\pm 1.0\%$) followed by cyclic tension-compression ($\varepsilon^p_x = \pm 1.0\%$) and opposite torsion ($\gamma^p_{xy}/\sqrt{3} = \pm 0.5\%$). a. The loading diagram. b. The yield surfaces in different moments of the loading history.

symmetrical to the τ_{xy}-axis (Fig. 12b-1 and Fig. 12b-2). Then, as the result of following cyclic $\varepsilon^p_x = \pm 0.5\%$ tension-compression it becomes symmetrical to the σ_x-axis and shrinks to its former magnitude (Fig. 12b-1 and Fig. 12b-3). Almost no memory effect is observed. Then, during the following cyclic opposite torsion loading ($\gamma^p_{xy}/\sqrt{3} = \pm 0.5\%$) it once

more becomes symmetrical to the τ_{xy}-axis. Its magnitude is almost the same as for the virgin $\gamma^p_{xy}/\sqrt{3} = \pm 0.5\%$ opposite torsion cyclic loading (Fig. 12b-4 and Fig. 12b-A).

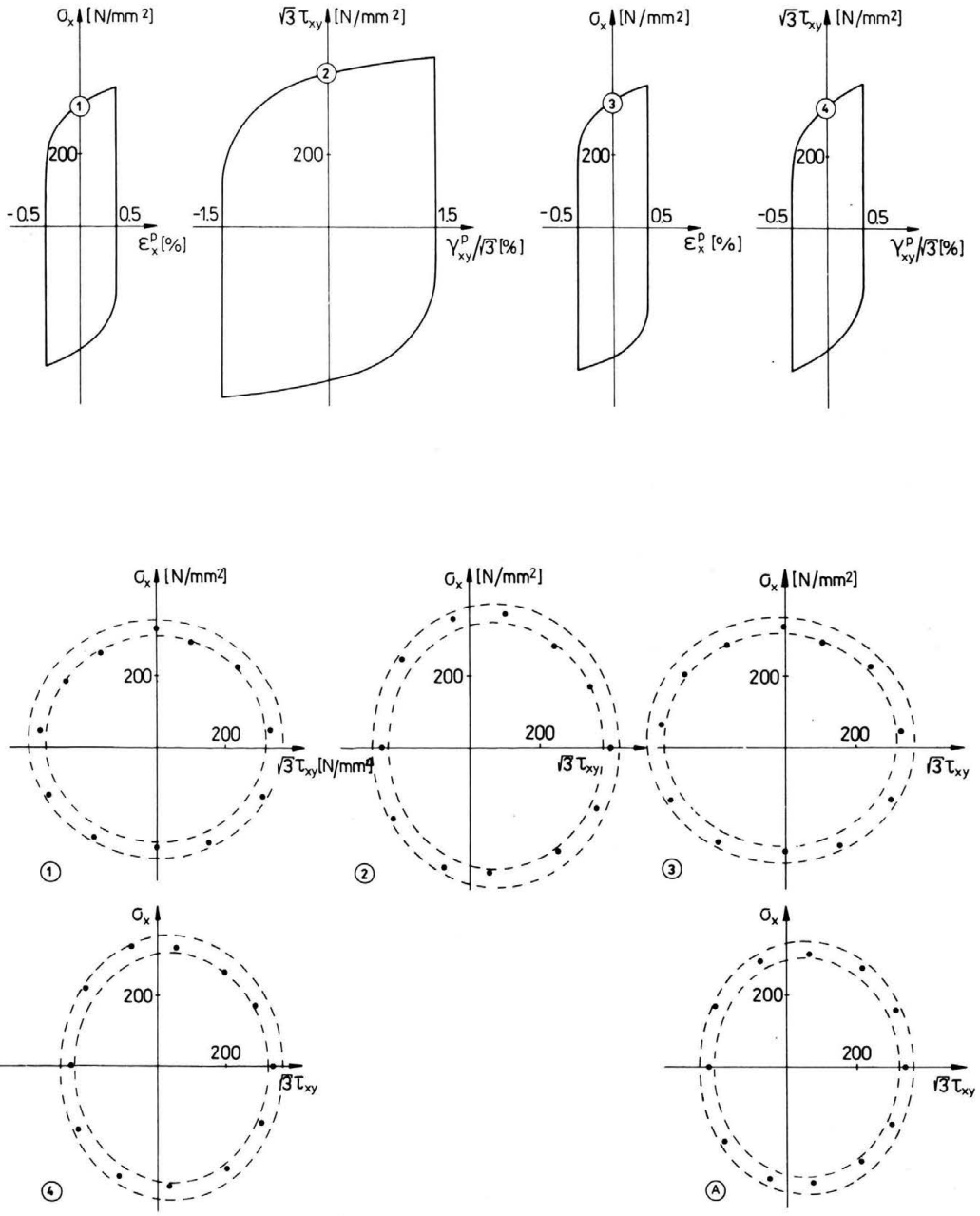

FIG. 12. Cyclic tension-compression ($\varepsilon^p_x = \pm 0.5\%$) followed by cyclic opposite torsion ($\gamma^p_{xy} = \pm 1.5\%$) and then cyclic tension compression and cyclic opposite torsion with this same amplitude ($\gamma^p_{xy}/\sqrt{3} = \pm 0.5\%$). a. The loading diagram. b. The yield surfaces measured in different moments of the loading history.

Experiment 7. Cyclic opposite torsion ($\gamma_{xy}^p/\sqrt{3} = \pm 0.5\%$) followed by cyclic tension-compression-torsion complex loading followed by cyclic opposite torsion ($\gamma_{xy}^p/\sqrt{3} = 0.5\%$)

The specimen was first cyclically loaded under opposite torsion ($\gamma_{xy}^p/\sqrt{3} = \pm 0.5\%$) up to the stabilized loop, then the tension-compression-torsion complex cyclic loading was applied in the way shown in Fig. 13a. It was followed by opposite torsion with the $\gamma_{xy}^p/\sqrt{3} = \pm 0.5\%$ amplitude. The yield surfaces were determined in three moments of the loading history mentioned above, and comparison between the yield surfaces was made (Fig. 13b). The yield surface resulting from the complex cyclic loading is greater than that for the $\gamma_{xy}^p/\sqrt{3} = \pm 0.5\%$ cyclic opposite torsion. As a result of following cyclic torsion ($\gamma_{xy}^p/\sqrt{3} = \pm 0.5\%$), it becomes symmetrical to the τ_{xy}-axis and shrinks to the former magnitude (Fig. 13b-1 and Fig. 13b-3). Almost no memory effect is observed.

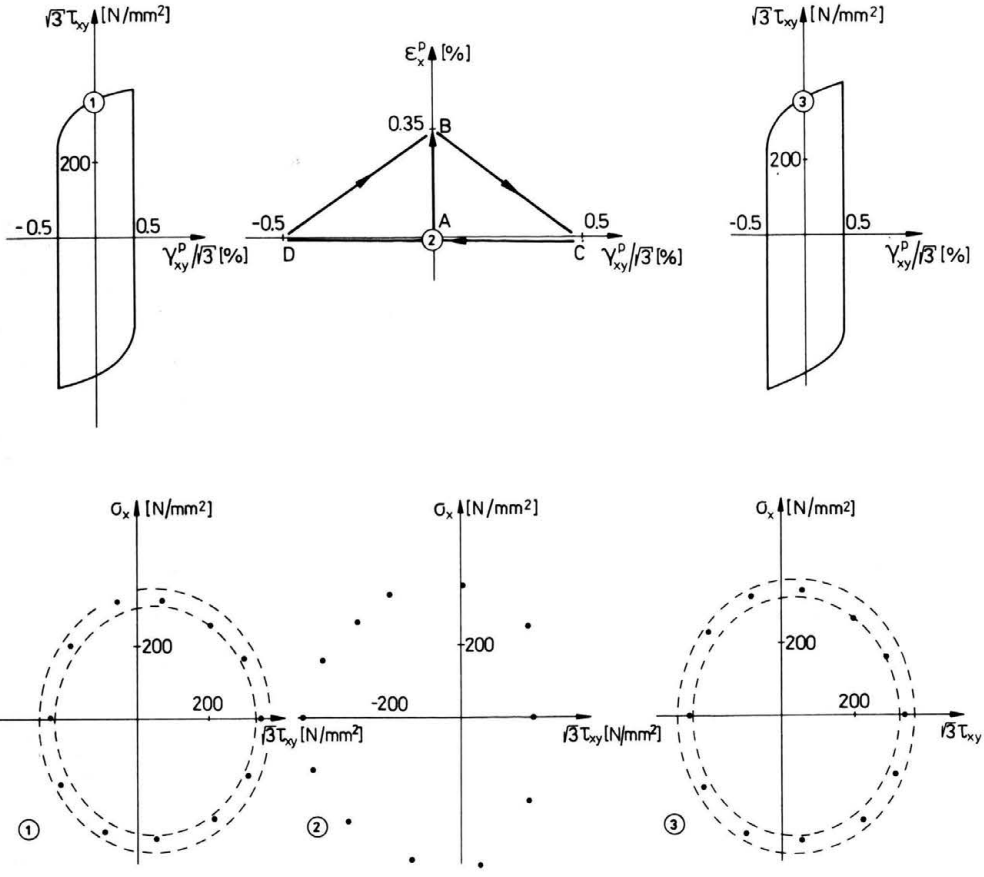

FIG. 13. Cyclic opposite torsion ($\gamma_{xy}^p/\sqrt{3} = \pm 0.5\%$) followed by cyclic tension-compression-torsion complex loading followed by cyclic opposite torsion ($\gamma_{xy}^p/\sqrt{3} = \pm 0.5\%$). a. The loading diagram. b. The yield surfaces measured in different moments of the loading history.

Experiment 8. Cyclic opposite torsion ($\gamma^p_{xy}/\sqrt{3} = \pm 0.5\%$ and $\gamma^p_{xy}/\sqrt{3} = \pm 1,0\%$) followed by cyclic tension-compression-torsion complex loading and cyclic opposite torsion ($\gamma^p_{xy}/\sqrt{3} = \pm 0.5\%$ and $\gamma^p_{xy}/\sqrt{3} = \pm 1.0\%$)

The loading program similar to that in Experiment 7 but for higher plastic amplitude complex loading was performed in Experiment 8. The specimen was first cyclically loaded under opposite torsion up to the stabilized loop with following strain amplitudes: $\gamma^p_{xy}/\sqrt{3} = \pm 0.5\%$ and $\gamma^p_{xy}/\sqrt{3} = \pm 1.0\%$. Then the tension-compression-torsion com-

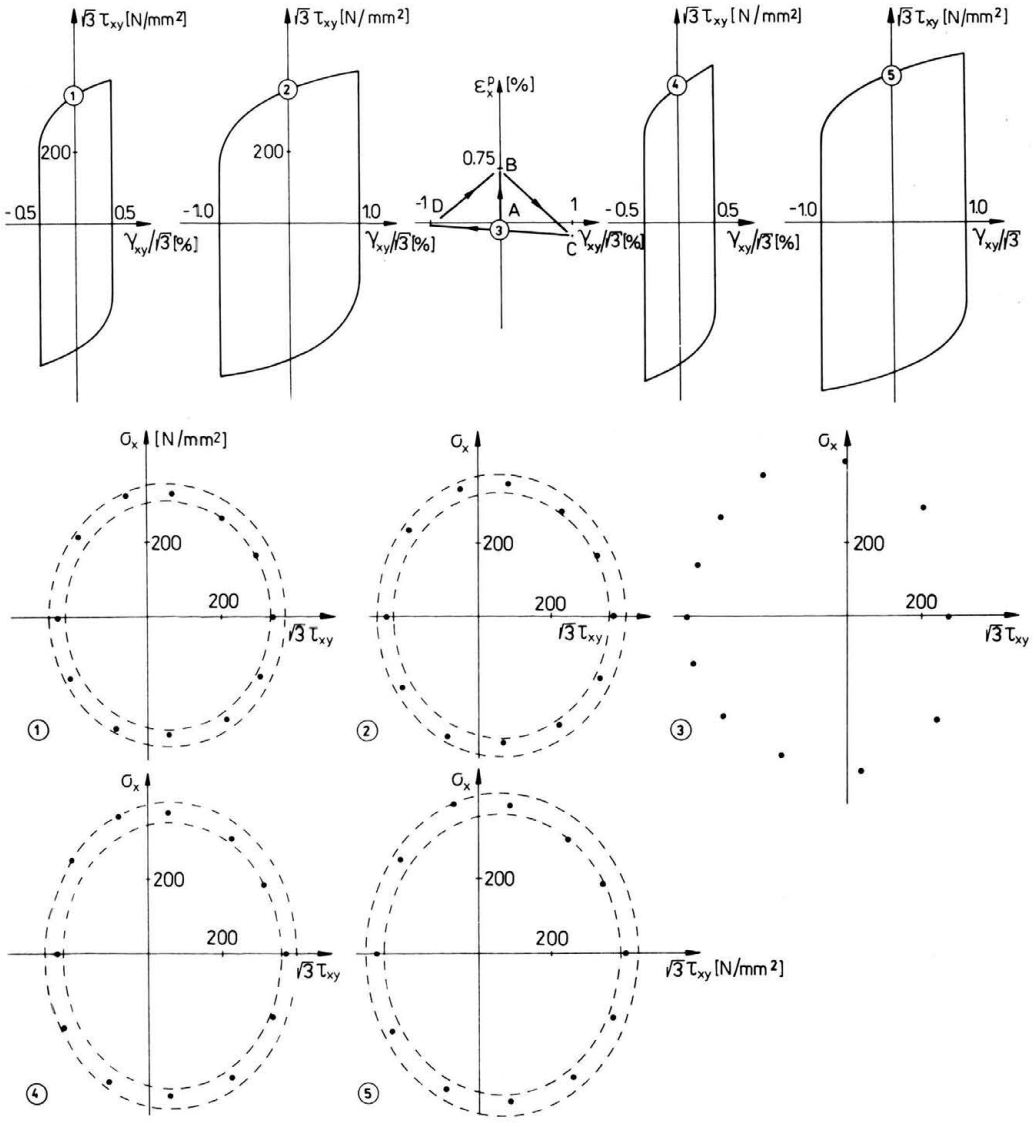

FIG. 14. Cyclic opposite torsion ($\gamma^p_{xy}/\sqrt{3} = \pm 0.5\%$ and $\gamma^p_{xy}/\sqrt{3} = \pm 1.0\%$) followed by cyclic tension-compression-torsion complex loading and cyclic opposite torsion ($\gamma^p_{xy}/\sqrt{3} = \pm 0.5\%$ and $\gamma^p_{xy}/\sqrt{3} = \pm 1.0\%$).

plex cyclic loading was applied in the way shown in Fig. 14a. It was followed by opposite torsion with the $\gamma^p_{xy}/\sqrt{3} = \pm 0.5\%$ and $\gamma^p_{xy}/\sqrt{3} = \pm 1.0\%$ amplitude. The yield surfaces were determined in five moments of the loading history mentioned above, and comparison between the yield surfaces was made (Fig. 14b). As before, the yield surface resulting from the complex cyclic loading is greater than that for the $\gamma^p_{xy}/\sqrt{3} = \pm 0.5\%$ and $\gamma^p_{xy}/\sqrt{3} = \pm 1.0\%$ cyclic opposite torsion. As a result of the following cyclic torsion ($\gamma^p_{xy}/\sqrt{3} = \pm 0.5\%$) it shrinks and becomes symmetrical to the τ_{xy}-axis, but its magnitude is larger than that for the virgin material opposite torsion (Fig. 14b-1 and Fig. 14b-4). Such memory effect (which results in the change of the yield surface magnitude while its shape remains almost constant) is observed also for the following opposite cyclic torsion with the $\gamma^p_{xy}/\sqrt{3} = \pm 1.0\%$ amplitude (Fig. 14b-2 and Fig. 14b-5).

Experiment 9. Cyclic opposite torsion ($\gamma^p_{xy}/\sqrt{3} = \pm 0.5\%$) with constant axial tension $\sigma_x = 50$ MPa

The specimen was cyclically loaded under cyclic opposite torsion ($\gamma^p_{xy}/\sqrt{3} = \pm 0.5\%$) with constant axial tension of $\sigma_x = 50$ MPa. The axial elongation was measured (Fig. 15a — ·····), and the yield surface was determined after 40 cycles (Fig. 15b-2). Comparing the shape of the yield surface with that for the virgin material cyclic opposite torsion (with this same amplitude $\gamma^p_{xy}/\sqrt{3} = \pm 0.5\%$ — the ellipse drawn by a solid line), it is seen that it points in the σ_x-direction. The surface is no longer symmetrical to the direction of loading.

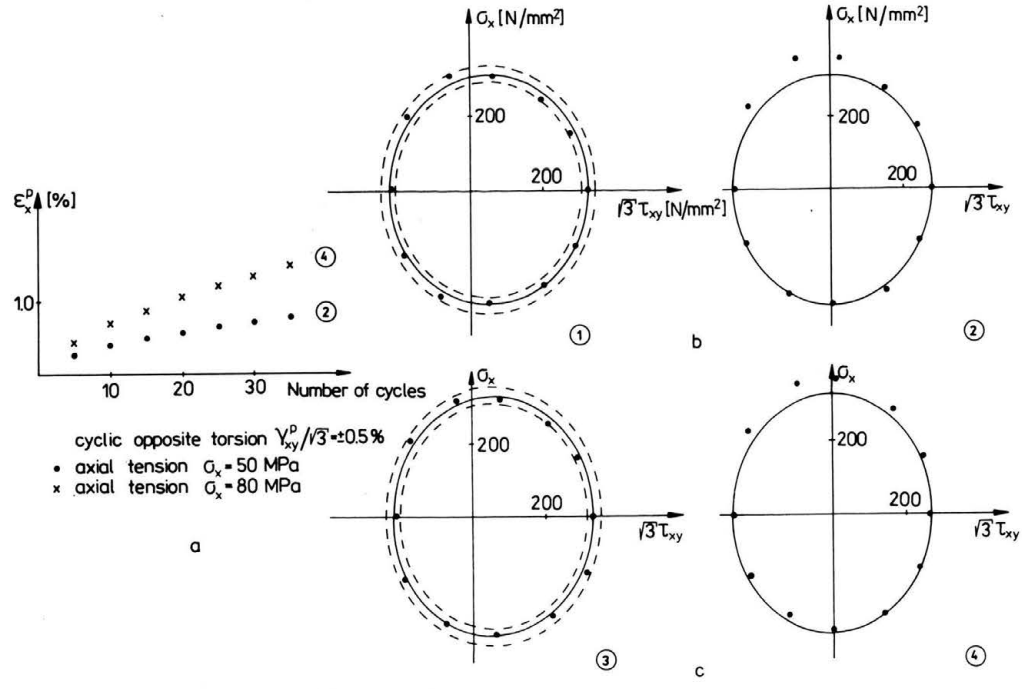

FIG. 15. Cyclic opposite torsion ($\gamma^p_{xy}/\sqrt{3} = \pm 0.5\%$) with constant axial tension. a. The axial elongation. b. 1–virgin material cyclic opposite torsion yield surface, 2–cyclic opposite torsion yield surface after 40 cycles when axial stress 50 MPa was applied. c. 1-virgin material cyclic opposite torsion yield surface, 2-cyclic opposite torsion yield surface after 40 cycles when axial stress 80 MPa was applied.

Experiment 10. Cyclic opposite torsion ($\gamma_{xy}^p/\sqrt{3} = \pm 0.5\%$) with constant axial tension $\sigma_x = 80$ MPa

An experimental program similar, to that reported in Experiment 9 was carried out in Experiment 10, but the axial tension $\sigma_x = 80$ MPa was applied. The axial elongation was measured (Fig. 15a – xxxxx), and the yield surface was determined after 40 cycles (Fig. 15b-4). As before, comparing the yield surface shape with that obtained for the virgin material cyclic opposite torsion (with the same amplitude $\gamma_{xy}^p/\sqrt{3} = \pm 0.5\%$ — the ellipse drawn by a solid line) it is seen that it points in σ_x-direction. The surface is no longer symmetrical to the direction of loading.

3. Conclusions

Taking into account the experimental results presented above and that presented in [11] the following conclusions can be drawn:

1. The yield surface, for the plastically strained material, doesn't coincide with the Huber–Mises surface and the significant cross-effect is observed.

2. The yield surfaces resulting from the proportional cyclic plastic loading and proportional monotonic loading flattens in the direction "opposite" to the actual plastic strains and gets a "nose" in the loading direction.

3. The surface has no longer the center of symmetry but it is symmetrical to the actual straining direction both in the case of monotonic proportional loading and in the case of steady state proportional cyclic loading. Such a behavior is independent of the former plastic strain history. The shape of the surface can be described, within the accuracy of $+8\%$, -6%, by an ellipse (in the assumed co-ordinate system).

4. The parameters describing two main yield surface dimensions (a, b) alternate simultaneously both in the case of proportional cyclic loading and in the case of proportional monotonic loading.

5. A certain memory effect is observed when the complex plastic loading is applied. It produces an increase of the magnitude of the cyclic steady state yield surface. The shape of the surface is similar to that for the virgin material.

6. The memory effect was also observed, when the monotonic prestrain was followed by cyclic loading with a small amplitude. As in point 5, it produces as the increase of the yield surface magnitude, but its shape is almost similar to that for the cyclic virgin material.

7. In the case of other loading histories, no memory effect was observed.

8. When the axial tension was applied during the opposite torsion loading (racheting — Fig. 15), the yield surface is drawn in σ_x direction. The surface is no longer symmetrical to the loading direction.

Acknowledgment

These experiments were carried out during W. Trąmpczyński's visit to Germany sponsored by the Alexander von Humboldt Foundation. The generosity of the Foundation, hospitality of the Institute of Mechanics I at the Bochum University and the assistance offered by prof. O. BRUHNS are gratefully acknowledged.

References

1. K. IKEGAMI, *Experimental plasticity on the anisotropy of metals*, Proc. Euromech Colloquium, 1979, [Ed.] J. BOEHLER, 115, 1982.
2. M. ŚLIWOWSKI, *Behavior of stress-strain diagrams for cyclic loading*, Bull. Acad. Polon. Sci., Série Sci. Tech., **27**, 115–123, 1979.
3. J. MIASTKOWSKI, W. SZCZEPIŃSKI, *An experimental study of yield surfaces for prestrained brass*, Int. J. Solids Struct., 1, 189–194, 1965.
4. A. PHILIPS, J. TANG, M. RICCIUTI, *Some new observations on yield surfaces*, Acta. Mech., **20**, 23–39, 1974.
5. H. ISHIKAWA, K. SASAKI, *Yield surfaces of SUS304 under cyclic loading*, J. Eng. Mat. and Techn., **110**, 364–371, 1988.
6. H. ISHIKAWA, K. SASAKI, *Stress strain relations of SUS304 stainless steel after cyclic preloading*, J. Eng. Mat. and Techn., vol. III, 417–423, 1989.
7. E. SHIRATORI, K. IKEGAMI, F. YOSIDA, S. KOIKE, *The subsequent yield surfaces after preloading under combined axial load and torsion*, Bull. Japan Soc. Mech. Eng., **19**, 134, 877–883, 1976.
8. W. SZCZEPIŃSKI, *On the effect of plastic deformations on yield conditions*, Arch. Mech. Stos., **15**, 275–293, 1963.
9. W. TRĄMPCZYŃSKI, *On a simple experimental technique for the yield surface determination*, Bull. Acad. Polon. Sci., Série Sci. Tech., **37**, 7–12, pp. 407–418, 1989.
10. X. WANG, A.S. KHAN and H. YAN, *On subsequent yield surfaces after finite shear pre-straining*, in: Anisotropy and Localisation of Plastic Deformation, Proceedings of Plasticity 91, [Ed.] J.P. BOEHLER and A.S. KHAN, Elsevier Applied Science, 1991.
11. W. TRĄMPCZYŃSKI, *The experimental verification of two points yield surface determination technique*, Arch. Mech., **44**, 2, 171–190, 1992.
12. TH. LEHMANN, B. RANIECKI and W. TRĄMPCZYŃSKI, *The Bauschinger effect in cyclic plasticity*, Arch. Mech., **37**, 6, 643– 659, 1985.
13. W. TRĄMPCZYŃSKI, *The experimental verification of the evolution of kinematic and isotropic hardening in cyclic plasticity*, J. Mech. Phys. Solids, **36**, 4, 417–441, 1988.

POLISH ACADEMY OF SCIENCES
INSTITUTE OF FUNDAMENTAL TECHNOLOGICAL RESEARCH.

Received April 14, 1992.